Exploiting Antenna Motion for Faster Initialization of Centimeter-Accurate GNSS Positioning with Low-Cost Antennas

Kenneth M. Pesyna, Jr.[1], *Student Member, IEEE*, Todd E. Humphreys[1], *Member, IEEE*, Robert W. Heath, Jr.[1], *Fellow, IEEE*, Thomas D. Novlan[2], *Member, IEEE*, and Jianzhong Charlie Zhang[2], *Senior Member, IEEE*

***Abstract*—This paper investigates the effectiveness of multipath-decorrelating antenna motion in reducing the initialization time of Global Navigation Satellite System (GNSS) receivers employing low-cost single-frequency antennas for carrier-phase differential GNSS (CDGNSS) positioning. Fast initialization times with low-cost antennas will encourage the expansion of CDGNSS into the mass market, bringing the benefits of globally-referenced centimeter-accurate positioning to many consumer applications, such as augmented reality and autonomous vehicles, that have so far been hampered by the several-meter-level errors of traditional GNSS positioning. Poor multipath suppression common to low-cost antennas results in large and strongly time-correlated phase errors when a receiver is static. Such errors can result in the CDGNSS initialization time, the so-called time to ambiguity resolution (TAR), extending to hundreds of seconds—many times longer than for higher-cost survey-grade antennas, which have substantially better multipath suppression. This paper demonstrates that TAR can be significantly reduced through gentle wavelength-scale random antenna motion. Such motion acts to decrease the correlation time of the multipath-induced phase errors. *A priori* knowledge of the motion profile is shown to further reduce TAR, with the reduction more pronounced as the initialization scenario is more challenging.**

I. Introduction

GNSS technology is present in nearly all smartphones and tablets, yet the underlying positioning accuracy of the consumer-grade GNSS receivers within them has stagnated over the past decade. The latest clock, orbit, and atmospheric models have improved receiver ranging accuracy to a meter or so [1], leaving receiver-dependent multipath as the dominant error source in current consumer devices [2]. Under good multipath conditions, 2-to-3-meter-accurate positioning is typical; under adverse multipath, accuracy degrades to 10 meters or worse.

Outside the mainstream of consumer GNSS receivers, however, centimeter-accurate GNSS positioning is routine. This level of accuracy, common in geodesy, agriculture, and surveying, results from replacing standard code-phase positioning techniques with carrier-phase differential GNSS (CDGNSS) techniques [3], [4]. Carrier phase techniques offer far more accurate positioning due to the much smaller wavelength of the GNSS signal's carrier, approximately 20 centimeters, as compared its spreading code, whose chip interval spans approximately 300 meters.

The primary impediment to performing centimeter-accurate CDGNSS positioning on smartphones and other consumer handheld devices lies not in the commodity GNSS chips, which actually outperform survey-grade chips in some respects [5]. Rather, it lies in the low-cost (e.g., a few cents to a few dollars), low-quality GNSS antennas, whose chief failing is poor multipath suppression. Multipath, caused by direct signals reflecting off the ground and nearby objects, induces centimeter-level phase measurement errors, which, for static receivers, have correlation times in the hundreds of seconds [6]. The time correlation of these errors, coupled with their relatively large magnitude, significantly increases the initialization period of GNSS receivers using low-cost antennas to achieve a centimeter-accurate CDGNSS positioning solution [7], [8], [9]. This is because, given a fixed measurement duration, a longer measurement error correlation time results in less information being provided to the CDGNSS estimator as it attempts to resolve the integer ambiguities inherent in CDGNSS processing, making their successful estimation less likely. Consequently, any strategy that reduces the measurement error correlation time—all else equal—leads to an increased ambiguity resolution success rate and thus a decreased initialization time, otherwise known as time to ambiguity resolution (TAR).

Prior work on mitigating the effect of correlated phase measurement errors in CDGNSS processing has focused not on decreasing the correlation time of the measurement errors, but on properly modeling time correlation within the CDGNSS estimator [10], [11], [12], [13]. While proper modeling leads to more accurate validation of integer ambiguity estimates, it does not significantly reduce—and can in some cases increase [13]—TAR.

This paper proposes gentle wavelength-scale random antenna motion as an effective strategy to reduce the correlation time of multipath-induced carrier phase errors, thus reducing TAR. Insofar as this paper's authors are aware, no prior work has advocated random antenna motion as a means to expedite CDGNSS ambiguity resolution. This is likely because, as this paper shows, antenna motion is beneficial—and practical—

This work was funded by Samsung Research America, The Data-Supported Transportation Operations and Planning Center (D-STOP), a Tier 1 USDOT University Transportation Center at The University of Texas at Austin, and the National Science Foundation under Grant Nos. 1454474 and NSF-CCF-1218338.

The authors are with [1]The University of Texas at Austin, Austin, TX 78712 USA and [2]Samsung Research America, Richardson, TX 75082 (email: kpesyna@utexas.edu, rheath@utexas.edu, todd.humphreys@mail.utexas.edu, jianzhong.z@samsung.com, t.novlan@samsung.com).

primarily for CDGNSS with small low-cost single-frequency antennas, which has been the subject of only recent study [7]. Single-frequency antennas are of primary focus because multi-frequency antennas—while offering more signals for increased ambiguity resolution performance—will for many years remain too expensive; they are at present hundreds of dollars too expensive for mass market products.

It may seem counterintuitive that antenna motion would lead to reduced TAR. However, this paper shows both by simulation and empirical study that for low-quality antennas, which experience relatively large phase measurement errors, the reduction in measurement error correlation time due to motion more than compensates for the increased dynamics uncertainty within a CDGNSS estimator. Conversely, it is shown that this is not the case for high-quality antennas. Moreover, it is demonstrated that TAR is further reduced with improved *a priori* knowledge of the antenna motion profile. In the limit of perfect motion profile knowledge, this paper's technique becomes similar to the synthetic aperture technique of [14], the difference being that [14] uses the perfect motion profile to coherently process the low-level complex GNSS correlation products, whereas this paper takes the slightly less optimal but simpler approach of operating on the usual carrier phase observables typically ingested by CDGNSS estimators.

The next section reviews existing multipath mitigation techniques and explains why they are largely ineffective or difficult to implement on low-cost, computationally-limited platforms. The following two sections detail models for the CDGNSS estimator and carrier phase multipath error. Subsequent sections analyze the effects of multipath on ambiguity resolution and investigate the benefits of antenna motion in reducing TAR.

II. Existing Multipath Mitigation Techniques

Existing techniques for mitigating GNSS carrier phase multipath tend to be unsuitable for low-cost platforms. Signal-processing-based techniques include the Multipath-Estimating Delay-Lock Loop [15], [16], a coupled multipath estimating phase-lock and delay-lock loop [17], signal-to-noise-ratio-based multipath error correction [18], the enhanced strobe correlator [19], and ray-tracing [20]. However, these techniques either require (1) precise, centimeter-accurate *a priori* knowledge of the motion profile of the GNSS antenna [17] and, in some cases, knowledge of the range and bearing of nearby reflection surfaces [20], (2) extra computational power to generate measurements at more than the usual number of correlator taps [15], [16], (3) a lengthy measurement duration, e.g., hundreds of seconds, for the correct identification of the multipath error frequency [18], or (4) a high sampling rate—in excess of 20 (real-valued) mega-samples per second [19].

Each of these enumerated requirements inhibits this paper's stated goal of fast centimeter positioning on low-cost, computationally limited platforms: (1) because a receiver will in most cases not have precise prior knowledge of its motion profile or of the relative position of nearby reflection surfaces; (2) because the platform is often computationally limited; (3) because hundreds of seconds of processing is too long; and (4) because a high sampling rate would add significant hardware cost to mass market receivers, whose narrow front-end bandwidth renders techniques such as that presented in [19] less effective [21]. Furthermore, many of these techniques have significantly reduced performance when the reflecting surface is less than about 10 meters from the receiving antenna [19], [16], a regime in which multipath-induced phase errors have been shown to be the largest [22].

Antenna-based multipath mitigation strategies, such as specially-designed groundplanes [23], [24] or antenna array solutions [25] are likewise inappropriate, as they require antenna setups that are at present far more expensive than the low-cost antennas that are this paper's focus.

This paper's exploration of random antenna motion for multipath mitigation is motivated by the inapplicability of existing multipath mitigation techniques to low-cost GNSS receivers.

III. CDGNSS Batch Estimator

The CDGNSS batch estimator employed in this paper takes as its input double-differenced (DD) carrier phase measurements made between two GNSS receivers, a reference and a rover, and processes these, together with a prior location estimate of the rover antenna center of motion and a model of the magnitude of variations about this center, to estimate (1) a centimeter-accurate relative position time history between the two receivers, and (2) a vector of carrier-phase integer ambiguities.

This paper employs batch estimation, as opposed to filtering, because batch estimation enables proper treatment of time correlation in the multipath-induced DD carrier phase measurement errors. Due to the estimator state's partial integer nature, state augmentation strategies typically employed to address time-correlated (colored) measurement errors in state estimation, such as those in [10], [26], actually weaken the mixed real-integer model, ultimately degrading the ambiguity resolution performance [13]. Batch estimation, by contrast, enables accurate and optimal treatment of measurement error time correlation in mixed real and integer estimation problems.

A. State

The batch estimator's state has a real-valued component that indirectly models the time-varying relative position between the reference and rover receiver, and an integer-valued component that models the so-called DD phase ambiguities. Such ambiguities are inherent in carrier phase differential positioning techniques; their resolution has been the topic of much past research [3], [27] and is required to produce a centimeter-accurate CDGNSS positioning solution.

Let k be the total number of measurement epochs input to the batch estimator and T be the time between consecutive epochs. The estimator's real-valued state component at $t_k = kT$, denoted $\mathbf{x}_k$, is given by

$$\mathbf{x}_k = [\mathbf{r}_C^\mathsf{T}, \mathbf{q}^\mathsf{T}, \mathbf{v}_0^\mathsf{T}, \ldots, \mathbf{v}_{k-1}^\mathsf{T}]^\mathsf{T}, \tag{1}$$

where

$\mathbf{r}_{\mathrm{C}}$ is the 3×1 constant relative position vector between the reference antenna and the center of motion of the rover antenna;

$\mathbf{q}$ is the 3×1 constant relative position vector between the rover antenna center of motion $\mathbf{r}_{\mathrm{C}}$ and the rover antenna initial relative position $\mathbf{r}_0$ at t_0, i.e., $\mathbf{r}_0 = \mathbf{r}_{\mathrm{C}} + \mathbf{q}$; and

$\mathbf{v}_i$ for $i = 0, 1, \ldots, k-1$ is a 3×1 vector proportional to the change in relative position between the reference and rover antenna from t_i to t_{i+1}. The exact relationship between $\mathbf{v}_i$ and the change in position is given in the next subsection.

The vectors $\mathbf{q}$ and $\mathbf{v}_i$, $i = 0, 1, \ldots, k-1$, are modeled as independent, zero-mean, Gaussian random vectors with variance σ_{p}^2:

$$\mathbf{q}, \mathbf{v}_i \sim \mathcal{N}(\mathbf{0}_{3\times 1}, \sigma_{\mathrm{p}}^2 \mathbf{I}_{3\times 3}),\ i = 0, 1, \ldots, k-1 \tag{2}$$

The estimator's integer-valued state component at t_k, denoted $\mathbf{n}_k$, given by

$$\mathbf{n}_k = [N_1, N_2, \ldots, N_{M_k - 1}]^{\mathsf{T}}, \tag{3}$$

where

M_k is the total number of satellites providing carrier phase measurements during at least one measurement epoch up to and including time t_k; and

N_i is the integer-valued phase ambiguity for the i^{th} satellite pair, $i = 1, 2 \ldots, M_k - 1$, assumed constant so long as both the reference and rover receivers retain phase lock on the signals tracked.

B. Relating the State to the Relative Rover Antenna Position

Let the rover antenna position relative to the reference antenna position at t_k be denoted $\mathbf{r}_k$. This vector sequence is assumed to evolve as an Ornstein-Uhlenbeck (OU) process—a mean-reverting first-order Gauss-Markov process. Such a process allows for adequate modeling of the time-correlated and mean-reverting motion a rover antenna would experience when moved randomly in the extended hand of an otherwise stationary user. Let $f = e^{-T/\tau_{\mathrm{p}}}$ be the correlation coefficient of the per-dimension time-varying changes in $\mathbf{r}_k$, where τ_{p} is the correlation time of these changes, in seconds. Under this model, $\mathbf{r}_k$ is related to the components of $\mathbf{x}_k$ by

$$\begin{aligned}
\mathbf{r}_0 &= \mathbf{r}_{\mathrm{C}} + \mathbf{q} \\
\mathbf{r}_k &= \mathbf{r}_{\mathrm{C}} + f\left(\mathbf{r}_{k-1} - \mathbf{r}_{\mathrm{C}}\right) + \sqrt{1 - f^2}\mathbf{v}_{k-1},\ k = 1, 2, \ldots \\
&= \mathbf{r}_{\mathrm{C}} + \sum_{i=0}^{k-1} f^{k-i}\left(\mathbf{q} + f^{-1}\sqrt{1-f^2}\mathbf{v}_i\right),\ k = 1, 2, \ldots
\end{aligned} \tag{4}$$

To adapt (4) to enforce a static antenna constraint, one can set the standard deviation of $\mathbf{q}$ and $\mathbf{v}_i$, $i = 0, 1, \ldots, k-1$, to zero, i.e., $\sigma_{\mathrm{p}} = 0$.

C. Measurement Model

The batch estimator's measurement model relates a time history of DD carrier phase measurements to the real- and integer-valued state components. The DD phase measurement at time $t_i \le t_k$ between satellites j and 1, with 1 denoting the common reference satellite, and the reference (A) and rover (B) receivers, is defined as

$$\phi_{\mathrm{AB},i}^{\mathrm{j1}} \triangleq \left[\phi_{\mathrm{A},i}^{\mathrm{j}} - \phi_{\mathrm{A},i}^{1}\right] - \left[\phi_{\mathrm{B},i}^{\mathrm{j}} - \phi_{\mathrm{B},i}^{1}\right], \tag{5}$$

for $j \in \{2, 3, \ldots, M_k\}$, and where $\phi_{\nu,i}^{\beta}$, $\nu \in \{\mathrm{A}, \mathrm{B}\}$, $\beta \in \{1, 2, \ldots, M_k\}$, is the undifferenced carrier phase measurement at t_i between receiver α and satellite β. As this paper's focus is multipath mitigation, the rover-reference pair is assumed to operate in the short-baseline regime for which atmospheric errors in the DD phase measurements are negligible. In this regime, $\phi_{\mathrm{AB},i}^{\mathrm{j1}}$, which has units of cycles, can be related to $\mathbf{r}_k$ and $\mathbf{n}_k$ by the following nonlinear measurement model [28]:

$$\lambda\phi_{\mathrm{AB},i}^{\mathrm{j1}} = r_{\mathrm{AB},i}^{\mathrm{j1}} + \lambda N_{j-1} + w_{\mathrm{AB},i}^{\mathrm{j1}} \tag{6}$$

where

$$r_{\mathrm{AB},i}^{\mathrm{j1}} \triangleq \left(r_{\mathrm{A},i}^{\mathrm{j}} - r_{\mathrm{A},i}^{1}\right) - \left(r_{\mathrm{B},i}^{\mathrm{j}} - r_{\mathrm{B},i}^{1}\right) \tag{7}$$

is the DD range between the two receivers and two satellites and

λ is the GNSS signal wavelength;

N_{j-1} is the integer ambiguity for the $(j-1)^{\mathrm{th}}$ satellite pair, as defined previously;

$w_{\mathrm{AB},i}^{\mathrm{j1}}$ is the DD carrier phase measurement error at t_i;

$r_{\alpha,i}^{\beta} \triangleq \|\mathbf{r}_i^{\beta} - \mathbf{r}_{\alpha,i}\|$, $\nu \in \{\mathrm{A}, \mathrm{B}\}$, $\beta \in \{1, 2, \ldots, M_k\}$, is the range between receiver α and satellite β at t_i, where $\|\cdot\|$ represents the Euclidean norm;

$\mathbf{r}_{\alpha,i}$ is the 3×1 absolute position of receiver $\nu \in \{\mathrm{A}, \mathrm{B}\}$ at t_i, the time of signal reception, in the global coordinate frame; and

$\mathbf{r}_i^{\beta}$ is the 3×1 absolute position of satellite $\beta \in \{1, 2, \ldots, M_k\}$ at the time of signal transmission, in the global coordinate frame.

Assuming that the position of the reference receiver is known and constant, i.e., $\mathbf{r}_{\mathrm{A},i} = \mathbf{r}_{\mathrm{A}}\ \forall i$, then (6) can be linearized about a guess $\bar{\mathbf{r}}_i$ of the relative rover position $\mathbf{r}_i \triangleq \mathbf{r}_{\mathrm{B},i} - \mathbf{r}_{\mathrm{A}}$, resulting in the linearized measurement model

$$\lambda\phi_{\mathrm{AB},i}^{\mathrm{j1}} = \bar{r}_{\mathrm{AB},i}^{\mathrm{j1}} + \mathbf{H}_{\mathrm{AB},i}^{\mathrm{j1}}(\mathbf{r}_i - \bar{\mathbf{r}}_i) + \lambda N_{j-1} + w_{\mathrm{AB},i}^{\mathrm{j1}}, \tag{8}$$

where $\bar{r}_{\mathrm{AB},i}^{\mathrm{j1}}$ is the DD range between the two receivers and satellites j and 1 assuming $\mathbf{r}_i = \bar{\mathbf{r}}_i$, and

$$\mathbf{H}_{\mathrm{AB},i}^{\mathrm{j1}} \triangleq \left.\frac{\partial r_{\mathrm{AB},i}^{\mathrm{j1}}}{\partial \mathbf{r}_i}\right|_{\mathbf{r}_i = \bar{\mathbf{r}}_i} = \left(\hat{\bar{\mathbf{r}}}_{\mathrm{B},i}^{1}\right)^{\mathsf{T}} - \left(\hat{\bar{\mathbf{r}}}_{\mathrm{B},i}^{j}\right)^{\mathsf{T}}$$

is the 1×3 linearized measurement sensitivity matrix, with $\hat{\bar{\mathbf{r}}}_{\mathrm{B},i}^{\beta}$ being the unit vector pointing from $\mathbf{r}_i^{\beta}$ to $\bar{\mathbf{r}}_{\mathrm{B},i} = \mathbf{r}_{\mathrm{A}} + \bar{\mathbf{r}}_i$, $\beta \in \{1, 2, \ldots, M_k\}$. Rewriting (8) with the known terms on the left and the unknown terms on the right results in the following, for $i = 1, 2, \ldots, k$:

$$\lambda\phi_{\mathrm{AB},i}^{\mathrm{j1}} - \bar{r}_{\mathrm{AB},i}^{\mathrm{j1}} + \mathbf{H}_{\mathrm{AB},i}^{\mathrm{j1}}\bar{\mathbf{r}}_i = \mathbf{H}_{\mathrm{AB},i}^{\mathrm{j1}}\mathbf{r}_i + \lambda N_{j-1} + w_{\mathrm{AB},i}^{\mathrm{j1}} \tag{9}$$

The estimator ingests, at t_k, $k = 1, 2, \ldots$, a $(M_k - 1)k \times 1$ vector $\mathbf{Y}_k$ of stacked inter-epoch measurement vectors from t_1 to t_k:

$$\mathbf{Y}_k \triangleq \begin{bmatrix} \mathbf{y}_1 \\ \mathbf{y}_2 \\ \vdots \\ \mathbf{y}_k \end{bmatrix} \tag{10}$$

where $\mathbf{y}_i$, $i = 1, 2, \ldots, k$, is an $(M_k - 1) \times 1$ vector containing the known quantities from the left-hand side of (9) at t_i for $j = 2, 3, \ldots, M_k$:

$$\mathbf{y}_i \triangleq \begin{bmatrix} \lambda\phi^{21}_{\mathrm{AB},i} - \bar{r}^{21}_{\mathrm{AB},i} + \mathbf{H}^{21}_{\mathrm{AB},i}\bar{\mathbf{r}}_i \\ \lambda\phi^{31}_{\mathrm{AB},i} - \bar{r}^{31}_{\mathrm{AB},i} + \mathbf{H}^{31}_{\mathrm{AB},i}\bar{\mathbf{r}}_i \\ \vdots \\ \lambda\phi^{M_k 1}_{\mathrm{AB},i} - \bar{r}^{\mathrm{j}1}_{\mathrm{AB},i} + \mathbf{H}^{M_k 1}_{\mathrm{AB},i}\bar{\mathbf{r}}_i \end{bmatrix}. \tag{11}$$

Using (9), it is now possible to linearly relate the real- and integer-valued state components in (1) and (3) to the DD carrier phase measurements in (10), incorporating the kinematics of the relative antenna position as modeled in (4). The linearized model becomes

$$\mathbf{Y}_k = \tilde{\mathbf{H}}_{\mathrm{x}k}\mathbf{C}_k\mathbf{x}_k + \tilde{\mathbf{H}}_{\mathrm{n}k}\mathbf{n}_k + \mathbf{W}_k, \tag{12}$$

where

- $\tilde{\mathbf{H}}_{\mathrm{x}k}$ is the time-dependent measurement sensitivity matrix for the real-valued state component $\mathbf{x}_k$ (expanded below);
- $\mathbf{C}_k$ is the time-dependent correlation matrix modeling the dynamics of the reference–rover three-dimensional relative position $\mathbf{r}_k$, as detailed in Sec. III-B (expanded below);
- $\tilde{\mathbf{H}}_{\mathrm{n}k}$ is the measurement sensitivity matrix for the integer-valued state component (expanded below);
- $\mathbf{W}_k$ is the discrete-time stacked DD measurement error vector, modeled as zero mean with covariance matrix $\mathbf{R}_k$, i.e., $\mathbf{E}[\mathbf{W}_k] = \mathbf{0}$ and $\mathbf{E}\left[\mathbf{W}_k\mathbf{W}_k^{\mathrm{T}}\right] = \mathbf{R}_k$ (expanded below).

$\tilde{\mathbf{H}}_{\mathrm{x}k}$, $\mathbf{C}_k$, $\tilde{\mathbf{H}}_{\mathrm{n}k}$, and $\mathbf{W}_k$ can be expanded as

$$\tilde{\mathbf{H}}_{\mathrm{x}k} \triangleq \begin{bmatrix} \mathbf{H}_{\mathrm{AB},1} & \mathbf{0} & \ldots & \mathbf{0} \\ \mathbf{0} & \mathbf{H}_{\mathrm{AB},2} & \ddots & \vdots \\ \vdots & & & \mathbf{0} \\ \mathbf{0} & \mathbf{0} & & \mathbf{H}_{\mathrm{AB},k} \end{bmatrix} \tag{13}$$

$$\mathbf{C}_k \triangleq \mathbf{I}_{3\times 3} \otimes \begin{bmatrix} 1 & f^0 & 0 & \ldots & \ldots & 0 \\ 1 & f^1 & af^0 & 0 & \ldots & 0 \\ \vdots & \vdots & \vdots & \ddots & \ddots & \vdots \\ 1 & f^{k-1} & af^{k-2} & \ldots & af^0 & 0 \\ 1 & f^k & af^{k-1} & \ldots & af^1 & af^0 \end{bmatrix} \tag{14}$$

$$\tilde{\mathbf{H}}_{\mathrm{n}k} \triangleq \begin{bmatrix} \lambda\mathbf{I}_{(\mathrm{M_k}-1)\times(\mathrm{M_k}-1)} \\ \lambda\mathbf{I}_{(\mathrm{M_k}-1)\times(\mathrm{M_k}-1)} \\ \vdots \\ \lambda\mathbf{I}_{(\mathrm{M_k}-1)\times(\mathrm{M_k}-1)} \end{bmatrix} \tag{15}$$

$$\mathbf{W}_k \triangleq \begin{bmatrix} \mathbf{w}_1 \\ \mathbf{w}_2 \\ \vdots \\ \mathbf{w}_k \end{bmatrix}, \tag{16}$$

where "$\otimes$" denotes the Kronecker product, f is the correlation coefficient of the time-varying reference–rover relative position changes, as introduced in (4), $a \triangleq \sqrt{1 - f^2}$,

$$\mathbf{w}_i \triangleq \begin{bmatrix} w^{21}_{\mathrm{AB},i} \\ w^{31}_{\mathrm{AB},i} \\ \vdots \\ w^{M_k 1}_{\mathrm{AB},i} \end{bmatrix}, \ i = 1, 2, \ldots, k$$

and

$$\mathbf{H}_{\mathrm{AB},i} \triangleq \begin{bmatrix} \mathbf{H}^{21}_{\mathrm{AB},i} \\ \mathbf{H}^{31}_{\mathrm{AB},i} \\ \vdots \\ \mathbf{H}^{M_k 1}_{\mathrm{AB},i} \end{bmatrix}, \ i = 1, 2, \ldots, k.$$

The measurement error covariance matrix $\mathbf{R}_k$ facilitates proper modeling of the magnitude and time correlation of the DD phase measurement errors, which, similar to the rover antenna position, are assumed to evolve as an OU process. $\mathbf{R}_k$ can be expanded as

$$\mathbf{R}_k \triangleq \mathbf{R}_\phi \otimes \mathbf{D}_k, \tag{17}$$

where

$$\mathbf{R}_\phi \triangleq \sigma^2_\phi \begin{bmatrix} 4 & 2 & \ldots & 2 \\ 2 & 4 & & \vdots \\ \vdots & & \ddots & 2 \\ 2 & \ldots & 2 & 4 \end{bmatrix} \tag{18}$$

models the *intra*-epoch measurement error correlation resulting from the presence of a common reference satellite in the DD measurements [see [4], Eq. (19)], and σ^2_ϕ is the average variance of the reference and rover antenna undifferenced phase error:

$$\sigma^2_\phi \triangleq \frac{\sigma^2_{\phi,\mathrm{A}} + \sigma^2_{\phi,\mathrm{B}}}{2}. \tag{19}$$

$\mathbf{D}_k$ models the *inter*-epoch measurement error correlation, i.e., the correlation in time. The measurement error time history for each DD satellite pair is modeled as an OU process, which is the simplest process that accurately models the time-correlated- and mean-reverting-nature of the DD phase errors. Choosing an OU process also simplifies the relationship between statistics of the antenna motion, also modeled as an OU process [see (4)], to the statistics of DD measurement errors, as will be detailed later on. $\mathbf{D}_k$ can be expanded as

$$\mathbf{D}_k \triangleq \begin{bmatrix} h(0) & h(1) & \ldots & h(k-1) \\ h(1) & h(0) & \ldots & h(k-2) \\ \vdots & \vdots & \vdots & \vdots \\ h(k-2) & h(k-3) & \ldots & h(1) \\ h(k-1) & h(k-2) & \ldots & h(0) \end{bmatrix}, \tag{20}$$

where $h(i)$ is the autocorrelation function of the DD reference and rover antenna phase errors, defined as

$$h(i) \triangleq \frac{\sigma^2_{\phi,\mathrm{A}} g^i_{\mathrm{A}} + \sigma^2_{\phi,\mathrm{B}} g^i_{\mathrm{B}}}{\sigma^2_{\phi,\mathrm{A}} + \sigma^2_{\phi,\mathrm{B}}}, \ i = 1, 2, \ldots, k, \tag{21}$$

and

$$g_{\mathrm{A}} \triangleq e^{-T/\tau_{\phi,\mathrm{A}}}$$
$$g_{\mathrm{B}} \triangleq e^{-T/\tau_{\phi,\mathrm{B}}}$$

are the correlation factors of the undifferenced rover and reference phase errors, which are modeled as exponentially decreasing with correlation times $\tau_{\phi,\mathrm{A}}$ and $\tau_{\phi,\mathrm{B}}$, respectively.

D. State Estimation

Optimal state estimates $\hat{\mathbf{x}}_k$ and $\hat{\mathbf{n}}_k$, $k = 1, 2, \ldots,$ are produced by incorporating all measurements and *a priori* information up to and including time t_k. A square-root information implementation of a batch estimator is employed for an accurate and computationally-efficient solution [29], [30].

A priori state information is provided to the estimator to enforce the models for $\mathbf{q}$ and $\mathbf{v}_i$, $i = 1, 2 \ldots, k$, detailed in (2), and to provide an approximation for the relative rover antenna center of motion $\mathbf{r}_{\mathrm{C}}$. This latter information is provided to the estimator in the form of a normalized square-root information equation:

$$\bar{\mathbf{z}}_{\mathrm{x}k} = \bar{\mathbf{R}}_{\mathrm{xx}k}\mathbf{x}_k + \bar{\mathbf{w}}_{\mathrm{x}k} \tag{22}$$

where

$\bar{\mathbf{z}}_{\mathrm{x}k} \triangleq \bar{\mathbf{R}}_{\mathrm{xx}k}\bar{\mathbf{x}}_k$ is the $3(k+2) \times 1$ nonhomogeneous term;

$\bar{\mathbf{x}}_k \triangleq \left[\bar{\mathbf{r}}_{\mathrm{C}}^{\mathsf{T}}, \mathbf{0}_{3\times1}^{\mathsf{T}}, \ldots, \mathbf{0}_{3\times1}^{\mathsf{T}}\right]$ is the prior estimate for the real-valued state component;

$\bar{\mathbf{R}}_{\mathrm{xx}k}$ is the square-root information matrix (SRIM) containing the prior information certainty corresponding to $\bar{\mathbf{x}}_k$ (expanded below); and

$\bar{\mathbf{w}}_{\mathrm{x}k}$ is the $3(k+2) \times 1$ error vector, modeled as zero mean with unit covariance, i.e., $\mathbf{E}\left[\bar{\mathbf{w}}_{\mathrm{x}k}\right] = \mathbf{0}_{3(\mathrm{k}+2)\times1}$ and $\mathbf{E}\left[\bar{\mathbf{w}}_{\mathbf{x}k}\bar{\mathbf{w}}_{\mathbf{x}k}^{\mathsf{T}}\right] = \mathbf{I}_{3(\mathrm{k}+2)\times3(\mathrm{k}+2)}$.

$\bar{\mathbf{R}}_{\mathrm{xx}k}$ is a block diagonal matrix, expanded as

$$\bar{\mathbf{R}}_{\mathrm{xx}k} \triangleq \begin{bmatrix} \frac{1}{\sigma_{\mathrm{r_C}}}\mathbf{I}_{3\times3} & \mathbf{0}_{3\times3} & \ldots & \mathbf{0}_{3\times3} \\ \mathbf{0}_{3\times3} & \frac{1}{\sigma_{\mathrm{p}}}\mathbf{I}_{3\times3} & \ldots & \mathbf{0}_{3\times3} \\ \vdots & \vdots & \ddots & \vdots \\ \mathbf{0}_{3\times3} & \mathbf{0}_{3\times3} & \ldots & \frac{1}{\sigma_{\mathrm{p}}}\mathbf{I}_{3\times3} \end{bmatrix}, \tag{23}$$

where $\sigma_{\mathrm{r_C}}$ is the per-dimension error standard deviation of $\bar{\mathbf{r}}_{\mathrm{C}}$, in meters.

The carrier phase measurements are also modeled by a normalized square-root information equation through the following transformation of $\mathbf{Y}_k$:

$$\mathbf{z}_k \triangleq \mathbf{R}_{\mathrm{a}k}^{-\mathsf{T}}\mathbf{Y}_k \tag{24}$$
$$= \mathbf{H}_{\mathrm{x}k}\mathbf{x}_k + \mathbf{H}_{\mathrm{n}k}\mathbf{n}_k + \mathbf{w}_k \tag{25}$$

where

$\mathbf{R}_{\mathrm{a}k} \triangleq \mathrm{chol}\left(\mathbf{R}_k\right)$ is the Choleski factorization, i.e., the inverse square root, of the measurement error covariance matrix $\mathbf{R}_k$;

$\mathbf{z}_k$ is the $k(M_k - 1) \times 1$ nonhomogeneous term corresponding to $\mathbf{x}_k$ and $\mathbf{n}_k$;

$\mathbf{H}_{\mathrm{x}k} \triangleq \mathbf{R}_{\mathrm{a}k}^{-\mathsf{T}}\tilde{\mathbf{H}}_{\mathrm{x}k}\mathbf{C}_k$ is the normalized measurement sensitivity matrix for the real-valued state component $\mathbf{x}_k$;

$\mathbf{H}_{\mathrm{n}k} \triangleq \mathbf{R}_{\mathrm{a}k}^{-\mathsf{T}}\tilde{\mathbf{H}}_{\mathrm{n}k}$ is the normalized measurement sensitivity matrix for the integer-valued state component $\mathbf{n}_k$; and

$\mathbf{w}_k \triangleq \mathbf{R}_{\mathrm{a}k}^{-\mathsf{T}}\mathbf{W}_k$ is the normalized measurement error, modeled as zero mean with unit covariance, i.e., $\mathbf{E}\left[\mathbf{w}_k\right] = \mathbf{0}_{\mathrm{k}(\mathrm{M_k}-1)\times1}$ and $\mathbf{E}\left[\mathbf{w}_k\mathbf{w}_k^{\mathsf{T}}\right] = \mathbf{I}_{\mathrm{k}(\mathrm{M_k}-1)\times\mathrm{k}(\mathrm{M_k}-1)}$.

Optimal estimates of the real- and integer-valued state elements can be found by choosing $\mathbf{x}_k$ and $\mathbf{n}_k$ to minimize the following cost function:

$$\begin{aligned} J\left(\mathbf{x}_k, \mathbf{n}_k\right) = &\Big\| \underbrace{\mathbf{H}_{\mathrm{x}k}\mathbf{x}_k + \mathbf{H}_{\mathrm{n}k}\mathbf{n}_k - \mathbf{z}_k}_{\text{Normalized Measurement Error}} \Big\|^2 \\ &+ \Big\| \underbrace{\bar{\mathbf{R}}_{\mathrm{xx}k}\mathbf{x}_k - \bar{\mathbf{z}}_{\mathrm{x}k}}_{\text{Normalized Prior Error}} \Big\|^2 \end{aligned} \tag{26}$$

where $\|\cdot\|$ represents the Euclidean norm. Eq. (26) can be written equivalently as

$$J\left(\mathbf{x}_k, \mathbf{n}_k\right) = \left\| \underbrace{\begin{bmatrix} \mathbf{H}_{\mathrm{x}k} & \mathbf{H}_{\mathrm{n}k} \\ \bar{\mathbf{R}}_{\mathrm{xx}k} & \mathbf{0} \end{bmatrix}}_{\mathbf{H}} \begin{bmatrix} \mathbf{x}_k \\ \mathbf{n}_k \end{bmatrix} - \underbrace{\begin{bmatrix} \mathbf{z}_k \\ \bar{\mathbf{z}}_{\mathrm{x}k} \end{bmatrix}}_{\mathbf{z}} \right\|^2. \tag{27}$$

By QR factorization [31], the block matrix $\mathbf{H}$ in (27) can be transformed into the product of a square, orthonormal matrix and an upper triangular matrix:

$$\mathbf{Z} = \mathbf{Q}_{\mathrm{b}}\mathbf{R}_{\mathrm{b}} \tag{28}$$

By left multiplying $\mathbf{H}$ and $\mathbf{z}$ of (27) by $\mathbf{Q}_{\mathrm{b}}^{\mathsf{T}}$, the cost function can be written equivalently as

$$J\left(\mathbf{x}_k, \mathbf{n}_k\right) = \left\| \begin{bmatrix} \mathbf{R}_{\mathrm{xx}k} & \mathbf{R}_{\mathrm{xn}k} \\ \mathbf{0} & \mathbf{R}_{\mathrm{nn}k} \\ \mathbf{0} & \mathbf{0} \end{bmatrix} \begin{bmatrix} \mathbf{x}_k \\ \mathbf{n}_k \end{bmatrix} - \begin{bmatrix} \mathbf{z}_{\mathrm{x}k} \\ \mathbf{z}_{\mathrm{n}k} \\ \mathbf{z}_{\mathrm{r}} \end{bmatrix} \right\|^2, \tag{29}$$

where

$\mathbf{R}_{\mathrm{xx}k}$ is the SRIM corresponding to $\mathbf{x}_k$ and $\mathbf{z}_{\mathrm{x}k}$;

$\mathbf{R}_{\mathrm{xn}k}$ is the SRIM corresponding to $\mathbf{n}_k$ and $\mathbf{z}_{\mathrm{x}k}$;

$\mathbf{z}_{\mathrm{x}k}$ is the nonhomogeneous term corresponding to $\mathbf{x}_k$ and $\mathbf{n}_k$;

$\mathbf{R}_{\mathrm{nn}k}$ is the SRIM corresponding to $\mathbf{n}_k$ and $\mathbf{z}_{\mathrm{n}k}$;

$\mathbf{z}_{\mathrm{x}k}$ is the nonhomogeneous term corresponding to $\mathbf{n}_k$; and

$\mathbf{z}_{\mathrm{r}}$ is the residual nonhomogeneous term.

This transformation leaves the cost in a convenient form that isolates a term involving only the integer-valued state component:

$$\begin{aligned} J\left(\mathbf{x}_k, \mathbf{n}_k\right) = &\underbrace{\left\|\mathbf{R}_{\mathrm{xx}k}\mathbf{x}_k + \mathbf{R}_{\mathrm{xn}k}\mathbf{n}_k - \mathbf{z}_{\mathrm{x}k}\right\|^2}_{\text{Term involving the integer- and real-valued states}} \\ &+ \underbrace{\left\|\mathbf{R}_{\mathrm{nn}k}\mathbf{n}_k - \mathbf{z}_{\mathrm{n}k}\right\|^2}_{\text{Term involving only the integer-valued state}} + \underbrace{\left\|\mathbf{z}_{\mathrm{r}}\right\|^2}_{\text{Residual term}} \end{aligned} \tag{30}$$

Minimization of (30) proceeds as follows: First, one finds, via efficient integer least-squares techniques [32], [27], the integer-valued vector state estimate $\hat{\mathbf{n}}_k$ that minimizes the second term on the right-hand side, the term involving only the integer-valued state. This is known as integer ambiguity resolution. Next, $\hat{\mathbf{n}}_k$ is inserted into the first term, the term involving both the integer- and real-valued states. At this point, it is possible to find the real-valued state estimate $\hat{\mathbf{x}}_k$ that reduces the first term to zero. By this process the state that minimizes $J\left(\mathbf{x}_k, \mathbf{n}_k\right)$ is found subject to an integer constraint on $\mathbf{n}_k$.

E. Phase Residuals

In addition to a time history of centimeter-accurate position estimates, the CDGNSS batch estimator outputs a time history of phase residuals $\tilde{\mathbf{Y}}_k$, which amount to departures of each DD phase measurement from phase alignment at the estimated phase center of the antenna. The vector of phase residuals is defined as

$$\tilde{\mathbf{Y}}_k \triangleq \mathbf{Y}_k - \mathbf{h}_k\left(\hat{\mathbf{x}}_k\right),$$

where

$$\mathbf{h}_k\left(\hat{\mathbf{x}}_k\right) \triangleq \begin{bmatrix} \mathbf{r}_{\mathrm{AB},1}\left(\hat{\mathbf{x}}_k\right) + \lambda \mathbf{I}_{(\mathrm{M_k}-1)\times(\mathrm{M_k}-1)}\hat{\mathbf{n}}_k \\ \mathbf{r}_{\mathrm{AB},2}\left(\hat{\mathbf{x}}_k\right) + \lambda \mathbf{I}_{(\mathrm{M_k}-1)\times(\mathrm{M_k}-1)}\hat{\mathbf{n}}_k \\ \vdots \\ \mathbf{r}_{\mathrm{AB},k}\left(\hat{\mathbf{x}}_k\right) + \lambda \mathbf{I}_{(\mathrm{M_k}-1)\times(\mathrm{M_k}-1)}\hat{\mathbf{n}}_k \end{bmatrix} \tag{31}$$

and

$$\mathbf{r}_{\mathrm{AB},i}\left(\hat{\mathbf{x}}_k\right) \triangleq \begin{bmatrix} r^{21}_{\mathrm{AB},i}\left(\hat{\mathbf{x}}_k\right) \\ r^{31}_{\mathrm{AB},i}\left(\hat{\mathbf{x}}_k\right) \\ \vdots \\ r^{\mathrm{M_k}1}_{\mathrm{AB},i}\left(\hat{\mathbf{x}}_k\right) \end{bmatrix}, \; i = 1, 2, \ldots, k. \tag{32}$$

The quantity $r^{\mathrm{j1}}_{\mathrm{AB},i}\left(\hat{\mathbf{x}}_k\right), \; j = 2, 3, \ldots, M_k$ is the DD range between satellites j and the reference satellite 1 at time t_i, which can be computed from the time-varying estimated reference-to-rover relative antenna position $\mathbf{r}_i$ and the position of the reference antenna $\mathbf{r}_{\mathrm{A}}$ using (7); $\mathbf{r}_i$ is derived from $\hat{\mathbf{x}}_k$ using using (4).

Phase residuals are examined in the next section to aid in motivating antenna motion as an effective strategy to improve the performance of CDGNSS integer ambiguity resolution.

IV. Carrier Phase Multipath Error Model

In the short-baseline CDGNSS regime (i.e., when the rover and reference antennas are separated by less than about 5 km), multipath errors remain substantial in DD carrier phase measurements whereas all other modeling errors are effectively cancelled by the DD operation detailed in (5) [33]. This explains why multipath errors are the primary impediment to fast carrier phase ambiguity resolution in the short-baseline regime [18], [34].

This section exploits an existing analytical model for carrier phase multipath to develop an approximate statistical relationship between (1) rover antenna quality and dynamics, and (2) carrier phase multipath errors. Subsequent sections will analyze ambiguity resolution performance in terms of multipath errors to complete the linkage from antenna quality and dynamics to ambiguity resolution success rate.

A. Single Reflection Multipath Error Model

Multipath-induced error in the phase estimates produced by a GNSS receiver's phase-locked loop as it tracks the carrier phase of a particular signal from a specific satellite can be approximated, in radians, by the following single-reflection error model [35]:

$$\psi \approx \arctan \frac{\alpha \sin\theta}{1 + \alpha\cos\theta}. \tag{33}$$

In this model, α is the power ratio and θ is the phase difference, in radians, between the reflected and line-of-sight (LOS) signals received by a GNSS antenna. Reflected signals are typically associated with low-elevation LOS signals and have significant non-right-hand-circularly-polarized (non-RHCP) components [36]. To attenuate reflected signals, high-quality antennas are designed to have a high axial ratio (a high level preference for RHCP) gain patterns that reject low-elevation signals. Because lower-quality antennas are worse in each of these properties, they attenuate signal reflections to a lesser extent. Thus, in the remainder of this paper, α is considered a proxy for reciprocal antenna quality, with α decreasing as antenna quality increases.

Although multipath commonly involves multiple reflections, the single-reflection model in (33) remains useful because errors can often be traced to a single dominant reflection [37]. The phase difference θ can be expanded as [20]

$$\theta = 2\pi\left(\frac{d_{\mathrm{ref}} - d_{\mathrm{los}}}{\lambda}\right), \tag{34}$$

where d_{ref} is the total distance traveled by the reflecting signal and d_{los} is the total distance traveled by the line-of-sight signal from the satellite to the receiving antenna, in meters. The next two subsections invoke (33) and (34) to illustrate how ψ is affected by satellite motion, receiver motion, and antenna quality.

B. Influence of Motion on Phase Errors

Carrier phase multipath has a spatial correlation on the order of one wavelength—approximately 19 centimeters at the GPS L1 frequency [38]. This spatial sensitivity has two important consequences: (1) multipath errors for each satellite signal are largely uncorrelated (between signals) at a particular location, and (2) the time correlation of errors for each signal is strongly influenced by receiver motion. The second of these consequences is further explained here.

Due to satellite motion, the difference $d_{\mathrm{ref}} - d_{\mathrm{los}}$, and, by extension, ψ, varies over time. For static antennas, ψ changes at a rate proportional to the distance between the receiving antenna and the closest reflecting surface [33], [20]. As most reflection surfaces are nearby (within 10 meters), carrier phase errors with correlation times in the hundreds of seconds are common [33], [6]. For moving antennas, ψ varies as a function of both satellite motion and receiver antenna motion. Due to the close proximity of the receiver antenna to the reflection surface, receiver motion—even compact wavelength-scale motion—induces significant changes to $d_{\mathrm{ref}} - d_{\mathrm{los}}$, and, by extension, to ψ.

To illustrate the influence of motion on phase errors, carrier phase data were captured from a smartphone-grade antenna both while the antenna was static and while it was moved in a quasi-random manner within a wavelength-scale volume. The data capture setup was as follows: (1) radio frequency (RF) signals were received through the smartphone's internal antenna, RF filters, and low-noise amplifier and were captured and digitized for external processing (see [39], Fig. 1, for further details); (2) data for the static antenna scenario were

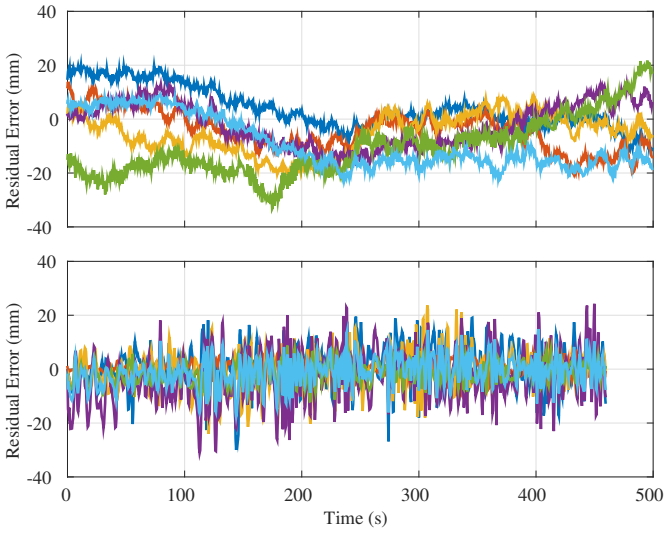

Fig. 1. Time histories of phase residuals for a batch of data captured from a smartphone-grade antenna while static (top panel) and while in motion (bottom panel). Each trace represents a DD phase residual history for a different satellite pair. A survey-grade antenna was used as the reference antenna, which remained static throughout the data capture interval.

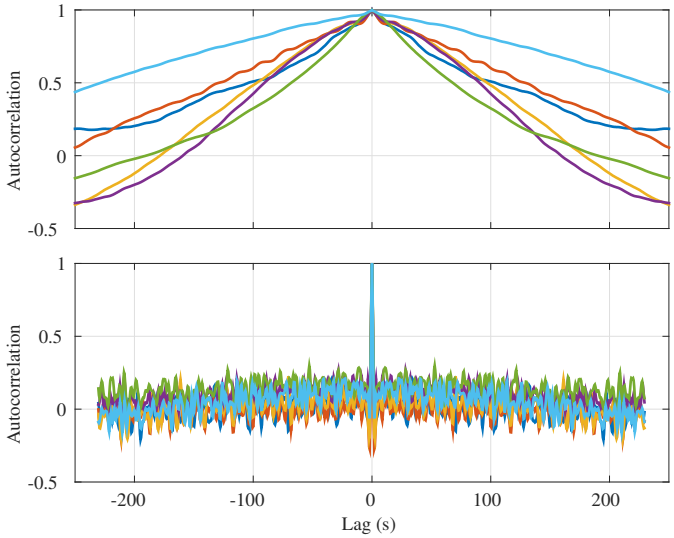

Fig. 2. Autocorrelation functions corresponding to the phase residuals in Fig. 1.

obtained while the phone rested on a flat plastic surface affixed to the top of a 2-meter tripod; (3) data for the dynamic antenna scenario were obtained while the smartphone was moved randomly in the outstretched hand of an otherwise stationary user. In both scenarios, the same set of satellites was tracked, as data were captured at nearly the same time and location.

Fig. 1 shows DD the phase residuals and Fig. 2 shows the corresponding autocorrelation functions for the static (top panels) and dynamic (bottom panels) scenarios. It is clear that the phase residuals transform from slowly-varying ($>$ 100-second correlation) when the antenna is static to quickly-varying (sub-second correlation) when the antenna is dynamic.

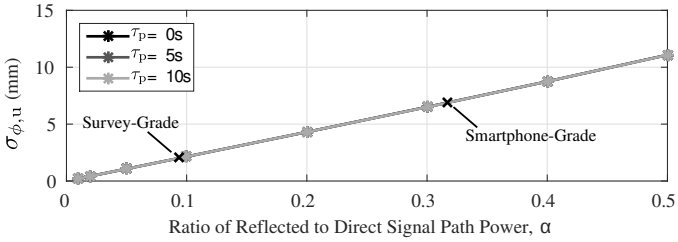

Fig. 3. Results of a Monte-Carlo-type simulation study showing the phase error standard deviation $\sigma_{\phi,\mathrm{u}}$ as a function of the antenna quality, characterized by α, and the correlation time of the antenna dynamics, characterized by τ_p. The traces for all three values of τ_p are coincident, indicating that $\sigma_{\phi,\mathrm{u}}$ does not depend on τ_p. The dependence of $\sigma_{\phi,\mathrm{u}}$ on α is approximately linear with the slope shown. Points along the $\sigma_{\phi,\mathrm{u}}(\alpha)$ trace corresponding to a survey-grade and smartphone-grade antenna have been marked. These are based on empirical values for $\sigma_{\phi,\mathrm{u}}$ [7].

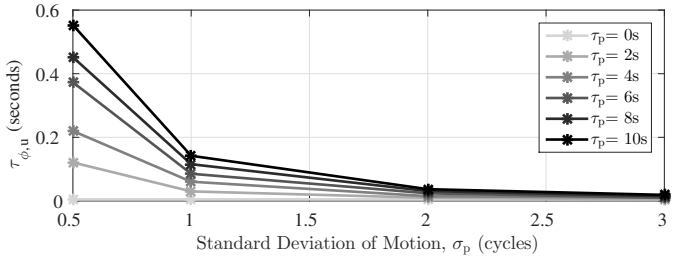

Fig. 4. Results of a Monte-Carlo-type simulation study showing the phase error correlation time $\tau_{\phi,\mathrm{u}}$ as a function of the standard deviation and correlation time of the antenna dynamics, σ_p and τ_p, respectively. It is clear that $\tau_{\phi,\mathrm{u}}$ decreases exponentially in σ_p and is approximately linear in τ_p.

C. Relationship between Antenna Quality and Dynamics and Phase Error Statistics

This section formalizes the relationship between antenna quality and dynamics, characterized by α, σ_p and τ_p, and the undifferenced phase error, characterized by either $\{\sigma_{\phi,\mathrm{B}}, \tau_{\phi,\mathrm{B}}\}$ or $\{\sigma_{\phi,\mathrm{A}}, \tau_{\phi,\mathrm{A}}\}$, the rover and reference antenna phase error statistics, respectively. Let w_α^β, for $\nu \in \{\mathrm{A},\mathrm{B}\}$, and $\beta \in \{1, 2, \ldots, M_k\}$ be the undifferenced contribution to the double differenced carrier phase measurement noise term $w_{\mathrm{AB},i}^{\mathrm{j1}}$ introduced in (8). Atmospheric and clock errors are ignored in w_α^β because they cancel in the double difference operation. Multipath errors are assumed to dominate the remaining carrier phase noise so that $w_\alpha^\beta \triangleq \psi$. The quantities $\{\sigma_{\phi,\mathrm{A}}, \tau_{\phi,\mathrm{A}}\}$ and $\{\sigma_{\phi,\mathrm{B}}, \tau_{\phi,\mathrm{B}}\}$ are thus interpreted as the standard deviation and time correlation of ψ for the respective antenna. For notational convenience in this section, $\{\sigma_{\phi,\mathrm{u}}, \tau_{\phi,\mathrm{u}}\}$ represents the generalized statistics of the undifferenced phase error, with u referring to either A or B.

Due to the strongly nonlinear nature of (33), the statistical relationship between phase errors and antenna quality and dynamics is difficult to define as closed-form expression. Instead, a Monte-Carlo-type simulation study was performed to approximate this relationship; the study's procedure is detailed in [40, Sec. 3.12.1]. Figures 3 and 4 indicate the significant relationships revealed by the study, which can be summarized as follows:

- $\sigma_{\phi,\mathrm{u}} \cong 21.9 \cdot \alpha$ for $0 \leq \alpha \leq 0.5$. A linear relationship is consistent with (33) for small α, since $\psi \to \alpha \sin\theta$ as

$\alpha \to 0$.

- $\tau_{\phi,\mathrm{u}} \cong 0.21 \cdot \tau_\mathrm{p} \cdot e^{-2.7\sigma_\mathrm{p}}$ for $0 \leq \tau_\mathrm{p} \leq 10$ seconds.
- $\sigma_{\phi,\mathrm{u}}$ does not depend significantly on σ_p or τ_p, and $\tau_{\phi,\mathrm{u}}$ does not depend on α.

The next section characterizes the dependence of CDGNSS integer ambiguity resolution on $\{\sigma_{\phi,\mathrm{u}}, \tau_{\phi,\mathrm{u}}\}$, so that, together with the results of this section, one can ultimately characterize ambiguity resolution performance in terms of antenna quality and dynamics.

V. Effect of Antenna Quality and Dynamics on Ambiguity Resolution

This paper's primary claim is that gentle wavelength-scale random antenna motion is an effective strategy to reduce TAR when performing a CDGNSS solution based on data collected from a low-quality antenna. Such motion improves the so-called ambiguity success rate (ASR), i.e., the probability that all integer ambiguities are successfully resolved, as compared to a static antenna CDGNSS solution. This section completes the linkage from $\{\alpha, \sigma_\mathrm{p}, \tau_\mathrm{p}\}$ to ASR and thus to TAR.

Previous work has developed closed-form expressions relating the undifferenced phase error statistics $\{\sigma_{\phi,\mathrm{u}}, \tau_{\phi,\mathrm{u}}\}$ to the so-called Ambiguity Dilution of Precision (ADOP) [41], [42], a scalar metric that can be used to compute a tight approximation of ASR [43]. These expressions, however, make one of two simplifying assumptions: they apply either under a short-time assumption, where phase error time correlation is considered but satellite motion is assumed negligible, or under a long-time assumption, where satellite motion is considered but phase error time correlation is assumed negligible. It does not appear possible to develop a closed-form approximation of ADOP which accounts for both satellite motion and error time correlation, yet it can be shown by simulation that both of these significantly affect ADOP, and thus ASR. Moreover, neither the short- nor long-term analytical expressions from [41], [42] account for the effect of receiver antenna trajectory uncertainty within the CDGNSS estimator on ASR.

A. Approach

This paper's approach is to employ Monte-Carlo simulation and the full batch CDGNSS estimator introduced in Sec. III, complete with a statistical antenna trajectory model, to determine the relationship between $\{\alpha, \sigma_\mathrm{p}, \tau_\mathrm{p}\}$ and ASR. The relationship is then validated with real data. The simulation study takes the following steps: (1) the values of $\{\alpha, \sigma_\mathrm{p}, \tau_\mathrm{p}\}$ given in Table I are used to generate a simulated rover antenna motion trajectory and are also mapped to corresponding values for $\tau_{\phi,\mathrm{u}}$ and $\sigma_{\phi,\mathrm{u}}$ using the model from Sec. IV; (2) the simulated antenna motion trajectory and the values for $\tau_{\phi,\mathrm{u}}$ and $\sigma_{\phi,\mathrm{u}}$ are used to generate simulated undifferenced carrier phase data for each satellite in the simulation; (3) the simulated carrier phase data are fed to the batch CDGNSS estimator to produce a series of batch solutions, and (4) analytical bounds on, and empirical estimates of, ASR are computed from the batch estimator's outputs after each measurement epoch; analytical bounds are computed using the estimator's state covariance matrix and empirical estimates are computed by comparing the batch estimator's integer ambiguity state estimate to the truth values. For all tests, the reference antenna is assumed to be survey-grade and static. Further details of the simulation study's procedure are found in [40, Sec. 3.12.2].

TABLE I
Model Parameters for Simulation Study of ASR

Motion Model				Quality		
	τ_p (sec)	σ_p (cycles)	$\tau_{\phi,\mathrm{u}}$ (sec)		α	$\sigma_{\phi,\mathrm{u}}$ (mm)
Static	n/a	0	100	Survey	0.09	2
Dynamic	2	0.5	0.12	Smartphone	0.32	7

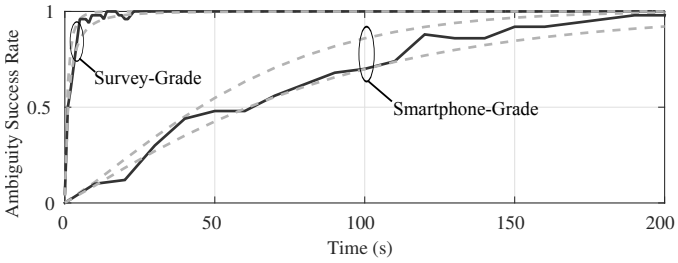

Fig. 5. ASR as a function of the total measurement time for two antenna grades: smartphone- and survey-grade. The dark solid traces denote the empirical estimate of ASR, obtained via Monte Carlo analysis, while the lighter dashed traces denote the analytically computed upper and lower bounds of ASR.

B. ASR Sensitivity to Antenna Quality

The simulation study considered survey- and smartphone-grade rover antennas, with the α values shown in Table I. The corresponding $\sigma_{\phi,\mathrm{u}}$ values characterize the magnitude of the simulated multipath-induced errors on the DD phase measurements. Both reference and rover antennas were assumed to be static for the study of ASR dependence on antenna quality. The results given in Fig. 5 show that the measured ASR (dark traces) closely track the upper and lower bounds (dashed traces) for each antenna type and that antenna quality strongly influences ASR, with the survey-grade antenna having a 90% TAR—the time required to reach an ASR exceeding 0.9—more than 10 times shorter than the smartphone-grade antenna.

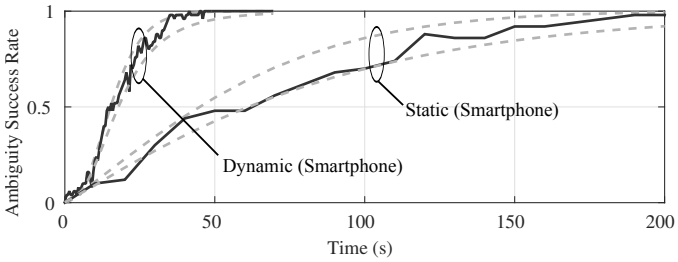

Fig. 6. ASR as a function of the total measurement time for a smartphone-grade rover antenna in two different dynamics scenarios. The dark solid traces denote the empirical estimate of ASR, obtained via Monte-Carlo simulation and analysis, while the lighter dashed traces denote the analytically computed upper and lower bounds of ASR.

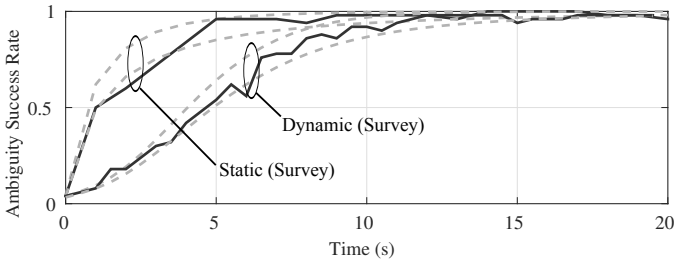

Fig. 7. As Fig. 6 but for a survey-grade rover antenna. Note the shorter time interval as compared to Fig. 6.

TABLE II
MODEL PARAMETERS FOR EMPIRICAL STUDY OF ASR

	Rover				Reference	
	τ_{p} (sec)	σ_{p} (cycles)	$\tau_{\phi,\mathrm{B}}$ (sec)	$\sigma_{\phi,\mathrm{B}}$ (mm)	$\tau_{\phi,\mathrm{A}}$ (sec)	$\sigma_{\phi,\mathrm{A}}$ (mm)
Static	n/a	0	300	6	100	2.5
Dynamic	1	1	0.01	6	100	2.5

C. ASR Sensitivity to Antenna Dynamics

The simulation study considered two rover antenna dynamics scenarios, static and gentle wavelength-scale random motion, labeled dynamic in Table I. The $\{\tau_{\mathrm{p}},\sigma_{\mathrm{p}}\}$ pairs for each scenario were mapped to $\tau_{\phi,\mathrm{u}}$ values characterizing the correlation time of the simulated multipath-induced errors on the DD phase measurements using the model from Sec. IV. Figs. 6 and 7 show the results for the smartphone- and survey-grade rover antennas, respectively.

For the smartphone antenna, antenna motion significantly reduces TAR. In this case, the information gained by more rapid phase decorrelation exceeded the information lost by not having a tight antenna position constraint. Comparison of Figs. 6 and 5 reveals that a moving smartphone-grade antenna can rival the TAR of a static survey-grade antenna. This is a significant result: it indicates that centimeter-accurate CDGNSS positioning on mass-market receivers can be made practically rapid. The result also holds, with even better TAR, for the next highest grade above smartphone-grade antennas, the low-quality patch antenna described in [39], though the static-to-dynamic improvement is not so drastic. The result is confirmed with real data in Sec. VI.

Interestingly, Fig. 7 reveals that motion lengthens TAR for a survey-grade rover antenna. It remains true that the phase measurement errors decorrelate more rapidly when the survey-grade antenna is moved, but because the magnitude of the phase errors is already so small, the information gained from faster phase error decorrelation does not compensate for the loss in information due to the added uncertainty (lack of constraint) in the motion model.

VI. ASR ANALYSIS USING REAL DATA

This section provides a demonstration using real data of the improvement to ASR that comes from motion for low-cost antennas.

A. Data Collection and Alignment

Raw digitized intermediate-frequency (IF) GPS L1 C/A data were collected simultaneously by two receivers, a reference and a rover. The reference antenna was a survey-grade Trimble Zephyr and the rover antenna was a low-cost Taoglas patch. 5000 seconds of static rover data were collected, followed immediately by 900 seconds of dynamic rover data. During the dynamic dataset the rover antenna was moved in a random, wavelength-scale, three-dimensional pattern while held in the hand of an otherwise stationary user. The 3-dimensional motion profile of the rover antenna can be approximately modeled as an OU process with the values for τ_{p} and σ_{p} found in the bottom row of Table II. The reference antenna remained stationary throughout data collection.

Each receiver ran a version of the GRID software-defined GNSS receiver [44], which processed the raw IF data and produced undifferenced code- and carrier-phase measurements. Each receiver's clock offset from GPS time was calculated at each measurement epoch from code phase measurements, enabling the carrier phase time histories to be timestamped in a common time base to approximately 15 ns accuracy. The rover's phase measurements were then interpolated to the time instants of the reference's measurements and the time histories were differenced according to (5) to form 7 DD carrier-phase time histories from the 8 highest elevation GPS satellites overhead at the time of the recording.

B. Phase Error Characterization

The carrier phase time histories produced from the recorded data exhibited errors whose statistics are summarized in Table II as $\{\tau_{\phi,\mathrm{B}},\ \sigma_{\phi,\mathrm{B}}\}$ and $\{\tau_{\phi,\mathrm{A}},\ \sigma_{\phi,\mathrm{A}}\}$ for the rover and reference antennas, respectively. These values were computed empirically from the DD residuals produced by CDGNSS batch processing over the full static and dynamic datasets. One exception is the value $\tau_{\phi,\mathrm{B}} = 0.01$ s for the dynamic dataset which, to avoid inaccuracy due to quantization effects, was calculated from the motion statistics τ_{p} and σ_{p} via the model in Sec. IV-C. The time correlation $\tau_{\phi,\mathrm{A}}$ is shorter than $\tau_{\phi,\mathrm{B}}$ because the reference antenna was further from reflecting surfaces than the rover antenna.

C. Data Processing

The DD carrier-phase time histories were split into 20 150-second and 12 65-second non-overlapping batches for the static and dynamic data sets, respectively. Each batch was provided separately to the CDGNSS estimator for processing along with the antenna motion and phase error statistics outlined in Table II. For each batch, the estimator output the following at each measurement epoch k (on the basis of the measurements ingested from epoch 0 to k): (1) an estimate of the integer-valued state $\hat{\mathbf{n}}_k$, and (2) the square-root information matrix $\mathbf{R}_{\mathrm{nn}k}$ denoting the filter's confidence in this integer-valued state estimate. Using these, empirical ASR and analytical ASR bounds were computed as described in [40, Sec. 3.12.2].

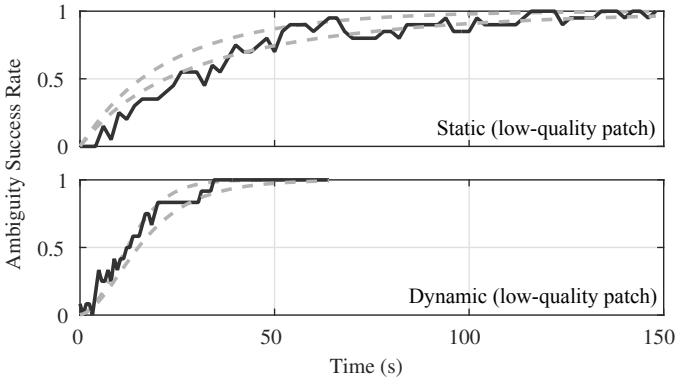

Fig. 8. ASR as a function of measurement time for two different antenna dynamics scenarios. The dark solid traces denote the empirical estimate of ASR, obtained from analysis of many disjoint real data intervals, while the lighter dashed traces denote the upper and lower ASR bounds, computed analytically based on the $\mathbf{R}_{\mathrm{nn}k}$ matrix.

D. Results

Fig. 8 plots ASR estimates and bounds as a function of measurement time for the two rover antenna dynamics scenarios characterized by the motion and phase error statistics in Table II. It is apparent that ASR performance improved with rover antenna motion; the time for ASR to reach 0.9, i.e., the 90% TAR, was reduced by over 50% for the dynamic vs. the static scenario.

VII. Ambiguity Resolution with a Provided Motion Profile

Previous sections have established that for low-quality antennas, antenna motion reduces TAR. In this case, the tradeoff between loss of information due to lack of a motion constraint and gain in information from more quickly decorrelating phase measurement errors favors motion. But if the moving antenna's precise motion profile were somehow provided to the estimator, there would be no tradeoff: the receiver would enjoy the more rapid error decorrelation without losing the motion constraint. Such a motion profile could be approximated from inertial sensors or from processing of images captured by a camera attached to the receiver, as in [**?**]. The profile may only be known to within a translation, rotation, or scale factor. In the limit of an error-free motion profile known to within a translation, the motion constraint becomes as effective as a static constraint.

Motion-profile-aided ambiguity resolution with inertially-derived trajectories has been shown to reduce the ambiguity search volume [45], but this earlier work did not characterize improvement in terms of TAR nor attempt demonstration with real data. Known motion profiles have also been used for multipath mitigation, whether to enable estimation of multipath parameters [17] or synthetic aperture processing [14]. The current paper's approach, described below, is similar to that of [14] except that it operates on the usual carrier phase observables instead of coherently processing the low-level correlation products.

A. Augmenting the CDGNSS Estimator with a Motion Profile

An *a priori* motion profile is incorporated into the CDGNSS estimator by augmenting the rover antenna relative position model of (4):

$$\mathbf{r}_k = \mathbf{r}_{\mathrm{C}} + \sum_{i=1}^{k} \mathbf{u}_i + \sum_{i=1}^{k} f^{k-i}\sqrt{1-f^2}\mathbf{v}_i \qquad (35)$$

where $\mathbf{u}_i$ is a 3×1 vector of the change in antenna position from t_{i-1} to t_i. Collectively, $\mathbf{u}_i$ for $i = 1, 2, \ldots, k$ form the *a priori* antenna motion profile. The real-valued state components $\mathbf{v}_i$ for $i = 1, 2, \ldots, k$ now model the changes to $\mathbf{r}_k$ from t_{i-1} to t_i not already captured by the *a priori* motion profile. Thus, the per-dimension standard deviation of $\mathbf{v}_i$, denoted σ_{p}, now models the uncertainty of $\mathbf{u}_i$ for $i = 1, 2, \ldots, k$.

Incorporating the augmented kinematic model of (35) into the batch estimator's measurement model results in the following augmented measurement model:

$$\mathbf{Y}_k - \mathbf{G}_k\mathbf{U}_k = \mathbf{H}_{\mathrm{x}k}\mathbf{C}_k\mathbf{x}_k + \mathbf{H}_{\mathrm{n}k}\mathbf{n}_k + \mathbf{W}_k \qquad (36)$$

where

$$\mathbf{U}_k \triangleq \begin{bmatrix} \mathbf{u}_1 \\ \mathbf{u}_2 \\ \vdots \\ \mathbf{u}_k \end{bmatrix} \qquad (37)$$

is a $3k \times 1$ vector containing the *a priori* knowledge of the change in antenna position from t_{i-1} to t_i for $i = 1, 2, \ldots, k$ and

$$\mathbf{G}_k = \begin{bmatrix} \mathbf{H}_{\mathrm{AB},1} & \mathbf{0} & \cdots & \mathbf{0} \\ \mathbf{H}_{\mathrm{AB},2} & \mathbf{H}_{\mathrm{AB},2} & \ddots & \vdots \\ \vdots & \vdots & \ddots & \mathbf{0} \\ \mathbf{H}_{\mathrm{AB},k} & \mathbf{H}_{\mathrm{AB},k} & & \mathbf{H}_{\mathrm{AB},k} \end{bmatrix} \qquad (38)$$

is the time-dependent lower-triangular measurement sensitivity matrix for $\mathbf{U}_k$.

B. Applying a Motion Profile to Real Data

An analysis of the TAR improvement offered by an *a priori* motion profile was performed with real data. The motion profile was obtained and was applied within the estimator as follows:

1) The absolute rover antenna three-dimensional trajectory was computed by performing a CDGNSS solution on the basis of the entire 900 second batch of dynamic data mentioned previously using phase measurements from all 12 satellites overhead at the time of the recording.
2) An unknown three-dimensional translation was added to the computed trajectory to obtain a translation-ambiguous motion profile. Such a translation ambiguity would also be present in a motion profile obtained using an inertial or vision system.
3) This motion profile was provided to the CDGNSS estimator in the form epoch-by-epoch antenna position changes, as the quantities $\mathbf{u}_i$, for $i \ldots k$ in (35). These vectors were

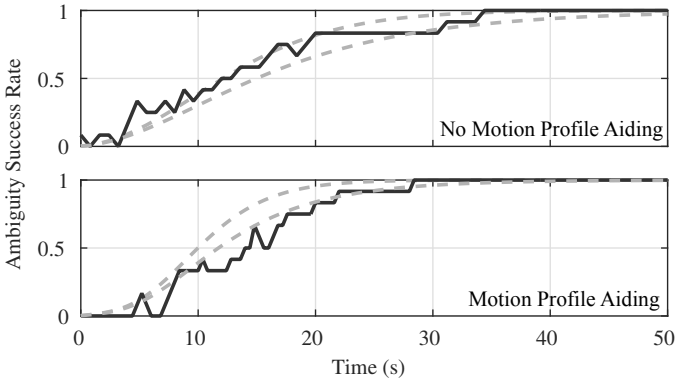

Fig. 9. ASR as a function of the total measurement time for a dynamic scenario without (top panel) and with (bottom panel) motion profile aiding. The dark solid traces denote the empirical estimate of ASR, while the lighter dashed traces denote the analytically-computed ASR upper and lower bounds.

stacked into a $3k \times 1$ vector $\mathbf{U}_k$ and integrated into the estimator's measurement model as in (36).

4) The assumed accuracy of the motion profile can be conveyed to the estimator through the statistics of the unknown receiver position, i.e., σ_{p} and τ_{p}. As the limiting case of a noise-free profile was most interesting for the current paper, it was assumed that $\sigma_{\mathrm{p}} = 0$ and $\tau_{\mathrm{p}} = \infty$.

C. Results

Fig. 9 shows that, for the data set studied, which is typical, motion profile aiding reduced the empirical 90% TAR by approximately 30%. The dark solid trace in the lower panel hangs below the ASR bounds because the motion profile was not, in fact, error free as the estimator was configured to assume. The bounds predict a reduction in 90% TAR for the error-free case of slightly more than 30%. Other tests revealed that the percent by which motion profile aiding improves TAR increases when there are fewer satellite signals available, i.e., when the initialization scenario is more challenging.

VIII. Conclusions

Using both simulated and empirical data it was shown that wavelength-scale random antenna motion is an effective strategy for significantly speeding integer ambiguity resolution when performing a CDGNSS solution using a low-cost GNSS antenna. Empirical resolution time was reduced by over 50% when the antenna was moved as compared to static. It was further shown that if *a priori* knowledge of the antenna's motion profile is available, such a constraint further reduces resolution time: an additional 30% reduction was shown for an empirical scenario in which a mm-accurate motion profile was known to within a translation. These results are significant: they portend an expansion of CDGNSS positioning into the mass market, where low-cost, low-quality antennas are abundant and CDGNSS initialization time is seen as a primary limiting factor.

References

[1] K. Alexander, "U.S. GPS program and policy update," in *26th SBAS International Working Group*. National Coordination Office, Feb. 2014.

[2] M. Sahmoudi and R. J. Landry, "Multipath mitigation techniques using maximum-likelihood principle," *Inside GNSS*, pp. 24–29, 2008.

[3] C. C. Counselman III, R. I. Abbot, S. A. Gourevitch, R. W. King, and A. R. Paradis, "Centimeter-level relative positioning with GPS," *Journal of Surveying Engineering*, vol. 109, no. 2, pp. 81–89, 1983.

[4] S. Mohiuddin and M. L. Psiaki, "High-altitude satellite relative navigation using carrier-phase differential global positioning system techniques," *Journal of Guidance, Control, and Dynamics*, vol. 30, no. 5, pp. 1628–1639, Sept.-Oct. 2007.

[5] F. van Diggelen, "Expert advice: Are we there yet? The state of the consumer industry," *GPS World*, Mar. 2010, GPS World.

[6] C. Miller, K. O'Keefe, and Y. Gao, "Time correlation in GNSS positioning over short baselines," *Journal of Surveying Engineering*, vol. 138, no. 1, pp. 17–24, 2011.

[7] K. M. Pesyna, Jr., R. W. Heath, Jr., and T. E. Humphreys, "Centimeter positioning with a smartphone-quality GNSS antenna," in *Proceedings of the ION GNSS+ Meeting*, 2014.

[8] C. Miller, K. OKeefe, and Y. Gao, "Operational performance of RTK positioning when accounting for the time correlated nature of GNSS phase errors," in *Proceedings of the ION GNSS Meeting*, 2010, pp. 21–24.

[9] K. O'Keefe, M. Petovello, G. Lachapelle, and M. E. Cannon, "Assessing probability of correct ambiguity resolution in the presence of time-correlated errors," *Navigation, Journal of the Institute of Navigation*, vol. 53, no. 4, pp. 269–282, 2007.

[10] M. G. Petovello, K. OKeefe, G. Lachapelle, and M. E. Cannon, "Consideration of time-correlated errors in a Kalman filter applicable to GNSS," *Journal of Geodesy*, vol. 83, no. 1, pp. 51–56, 2009.

[11] S. Han and C. Rizos, "Standardization of the variance-covariance matrix for GPS rapid static positioning," *Geomat. Res. Aust.*, vol. 62, pp. 37–54, 1995.

[12] P. Teunissen, "GPS ambiguity resolution: impact of time correlation, cross-correlation and satellite elevation dependence," *Studia Geophysica et Geodaetica*, vol. 41, no. 2, pp. 181–195, 1997.

[13] B. Li, S. Verhagen, and P. J. Teunissen, "Robustness of GNSS integer ambiguity resolution in the presence of atmospheric biases," *GPS Solutions*, vol. 18, no. 2, pp. 283–296, 2014.

[14] T. Pany, N. Falk, B. Riedl, C. Stber, J. Winkel, and H.-P. Ranner, "GNSS synthetic aperture processing with artificial antenna motion," in *Proceedings of the ION GNSS+ Meeting*. Nashville, Tennessee: Institute of Navigation, 2013.

[15] R. van Nee, J. Siereveld, P. Fenton, and B. Townsend, "The multipath estimating delay lock loop: approaching theoretical accuracy limits," in *Proceedings of the IEEE/ION PLANS Meeting*. IEEE, 1994, pp. 246–251.

[16] B. Townsend, P. Fenton, K. Van Dierendonck, and R. Van Nee, "L1 carrier phase multipath error reduction using MEDLL technology," in *Proceedings of the ION GPS Meeting*, vol. 8. INSTITUTE OF NAVIGATION, 1995, pp. 1539–1544.

[17] M. L. Psiaki, T. Ertan, B. W. O'Hanlon, and S. P. Powell, "GNSS multipath mitigation using antenna motion," *Navigation, Journal of the Institute of Navigation*, vol. 62, no. 1, pp. 1–22, 2015.

[18] P. Axelrad, C. J. Comp, and P. F. MacDoran, "SNR-based multipath error correction for GPS differential phase," *IEEE Transactions on Aerospace and Electronic Systems*, vol. 32, no. 2, pp. 650–660, 1996.

[19] L. Garin and J.-M. Rousseau, "Enhanced strobe correlator multipath rejection for code & carrier," in *Proceedings of the ION GPS Meeting*, 1997, pp. 559–568.

[20] L. Lau and P. Cross, "Development and testing of a new ray-tracing approach to GNSS carrier-phase multipath modelling," *Journal of Geodesy*, vol. 81, no. 11, pp. 713–732, 2007.

[21] M. S. Braasch, "Performance comparison of multipath mitigating receiver architectures," in *Aerospace Conference, 2001, IEEE Proceedings.*, vol. 3. IEEE, 2001, pp. 3–1309.

[22] C. Mekik and O. Can, "An investigation on multipath errors in real time kinematic GPS method," *Scientific Research and Essays*, vol. 5, no. 16, pp. 2186–2200, 2010.

[23] J. Tranquilla, J. Carr, and H. M. Al-Rizzo, "Analysis of a choke ring groundplane for multipath control in global positioning system (gps) applications," *IEEE Transactions on Antennas and Propagation*, vol. 42, no. 7, pp. 905–911, 1994.

[24] W. Kunysz, "High performance GPS pinwheel antenna," in *Proceedings of the ION International Technical Meeting*, 2000, pp. 19–22.

[25] J. Ray, M. Cannon, and P. Fenton, "GPS code and carrier multipath mitigation using a multiantenna system," *IEEE Transactions on Aerospace and Electronic Systems*, vol. 37, no. 1, pp. 183–195, 2001.

[26] Y. Bar-Shalom, X. R. Li, and T. Kirubarajan, *Estimation with Applications to Tracking and Navigation*. New York: John Wiley and Sons, 2001.

[27] P. Teunissen, P. De Jonge, and C. Tiberius, "The LAMBDA method for fast GPS surveying," in *Proceedings of International Symposium on GPS Technology Applications*, vol. 29. Bucharest, Romania: Union of Romanian Geodesy, Sept. 1995, pp. 203–210.

[28] M. Psiaki and S. Mohiuddin, "Modeling, analysis, and simulation of GPS carrier phase for spacecraft relative navigation," *Journal of Guidance Control and Dynamics*, vol. 30, no. 6, p. 1628, 2007.

[29] G. J. Bierman, *Factorization Methods for Discrete Sequential Estimation*. New York: Academic Press, 1977.

[30] M. Psiaki, "Kalman filtering and smoothing to estimate real-valued states and integer constants," *Journal of Guidance, Control, and Dynamics*, vol. 33, no. 5, pp. 1404–1417, Sept.-Oct. 2010.

[31] P. E. Gill, W. Murray, and M. H. Wright, *Practical optimization*. Academic press, 1981.

[32] K. M. Pesyna, Jr., Z. M. Kassas, R. W. Heath, Jr., and T. E. Humphreys, "A phase-reconstruction technique for low-power centimeter-accurate mobile positioning," *IEEE Transactions on Signal Processing*, vol. 62, no. 10, pp. 2595–2610, May 2014.

[33] J. Ray and M. Cannon, "Characterization of GPS carrier phase multipath," in *Proceedings of the ION National Technical Meeting*, 1999.

[34] D. F. Bétaille, P. A. Cross, and H.-J. Euler, "Assessment and improvement of the capabilities of a window correlator to model GPS multipath phase errors," *IEEE Transactions on Aerospace and Electronic Systems*, vol. 42, no. 2, pp. 705–717, 2006.

[35] J. J. Spilker, Jr., *Global Positioning System: Theory and Applications*. Washington, D.C.: American Institute of Aeronautics and Astronautics, 1996, ch. 14: Multipath Effects, pp. 547–568.

[36] V. U. Zavorotny, K. M. Larson, J. J. Braun, E. E. Small, E. D. Gutmann, and A. L. Bilich, "A physical model for GPS multipath caused by land reflections: Toward bare soil moisture retrievals," *Selected Topics in Applied Earth Observations and Remote Sensing, IEEE Journal of*, vol. 3, no. 1, pp. 100–110, 2010.

[37] P. Closas, C. Fernandez-Prades, and J. A. Fernandez-Rubino, "A Bayesian approach to multipath mitigation in GNSS receivers," *IEEE Journal of Selected Topics in Signal Processing*, vol. 3, no. 4, pp. 695–706, Aug. 2009.

[38] S. N. Sadrieh, A. Broumandan, and G. Lachapelle, "Spatial/temporal characterization of the GNSS multipath fading channels," in *Proceedings of the ION GNSS Meeting*, 2010, pp. 393–401.

[39] K. M. Pesyna, Jr, R. W. Heath, Jr., and T. E. Humphreys, "Accuracy in the palm of your hand: Centimeter positioning with a smartphone-quality GNSS antenna," *GPS World*, vol. 26, no. 2, pp. 16–31, Feb. 2015.

[40] K. M. Pesyna, Jr., "Advanced techniques for centimeter-accurate GNSS positioning on low-cost mobile platforms," Ph.D. dissertation, The University of Texas at Austin, Aug. 2015.

[41] P. J. Teunissen and D. Odijk, "Ambiguity dilution of precision: definition, properties and application," *Proceedings of ION GPS-1997*, pp. 16–19, 1997.

[42] D. Odijk and P. Teunissen, "Sensitivity of ADOP to changes in the single-baseline GNSS model," *Artificial Satellites*, vol. 42, no. 2, pp. 71–96, 2007.

[43] S. Verhagen, "On the reliability of integer ambiguity resolution," *Navigation, Journal of the Institute of Navigation*, vol. 52, no. 2, pp. 99–110, 2005.

[44] T. E. Humphreys, J. Bhatti, T. Pany, B. Ledvina, and B. O'Hanlon, "Exploiting multicore technology in software-defined GNSS receivers," in *Proceedings of the ION GNSS Meeting*. Savannah, GA: Institute of Navigation, 2009, pp. 326–338.

[45] J. Skaloud, "Reducing the GPS ambiguity search space by including inertial data," in *Proceedings of the ION International Technical Meeting*, 1998, pp. 2073–2080.